Chinese Chemical Letters 33 (2022) 2091–2095

Contents lists available at ScienceDirect

Chinese Chemical Letters

journal homepage: www.elsevier.com/locate/cclet

A lab-on-a-disc platform based on nickel nanowire net and smartphone imaging for rapid and automatic detection of foodborne bacteria

Xiaoting Huo[a,1], Lei Wang[a,1], Wuzhen Qi[b], Na Rong[b], Yingjia Liu[a], Siyuan Wang[b], Hong Duan[b], Jianhan Lin[a,b,*]

[a] Key Laboratory of Agricultural Information Acquisition Technology, Ministry of Agriculture and Rural Affairs, China Agricultural University, Beijing 100083, China

[b] Key Laboratory of Modern Precision Agriculture System Integration Research, Ministry of Education, China Agricultural University, Beijing 100083, China

ARTICLE INFO

Article history:
Received 31 May 2021
Revised 4 August 2021
Accepted 6 August 2021
Available online 12 August 2021

Keywords:
Lab-on-a-disk platform
Nickel nanowire net
Horseradish peroxidase nanoflowers
Smartphone
Bacteria detection

ABSTRACT

Foodborne pathogenic bacteria have been considered as a major risk factor for food safety. It is of great significance to carry out in-field screening of pathogenic bacteria to prevent the outbreaks of foodborne diseases. In this study, a portable lab-on-a-disc platform with a microfluidic disc was developed for rapid and automatic detection of *Salmonella typhimurium* using a nickel nanowire (NiNW) net for effective separation of target bacteria, horseradish peroxidase nanoflowers (HRP NFs) for efficient amplification of biological signals, and a self-developed smartphone APP for accurate analysis of colorimetric images. First, the microfluidic disc was preloaded with reagents and samples and centrifuged to form one bacterial sample column, one immune NiNW column, one HRP NF column, two washing buffer columns and one tetramethylbenzidine (TMB) column, which were separated by air gaps. Then, a rotatable magnetic field was specifically developed to assemble the NiNWs into a net, which was automatically controlled by a stepped motor to successively pass through the sample column for specific capture of target bacteria, the HRP NF column for specific label of target bacteria, the washing columns for effective removal of sample background and non-specific binding NFs, and the TMB column for colorimetric determination of target bacteria. The color change of TMB from colorless to blue was finally analyzed using the smartphone APP to quantitatively determine the target bacteria. This lab-on-a-disc platform could detect *Salmonella typhimurium* from 5.6×10^1 CFU/20 μL to 5.6×10^5 CFU/20 μL in 1 h with a lower detection limit of 56 CFU/20 μL. The recovery of target bacteria in spiked chicken samples ranged from 97.5% to 101.8%. This portable platform integrating separation, labeling, washing, catalysis and detection onto a single disc is featured with automatic operation, fast reaction, and small size and has shown its potential for in-field detection of foodborne pathogens.

Food safety is closely related to the public health. According to the report of the World Bank, foodborne diseases have resulted in an annual productivity loss of ~$95.2 billion and an annual medical expense of ~$15 billion in low and middle-income countries [1]. Around 600 million people fall ill with 420,000 deaths every year in the world after eating unsafe foods containing harmful bacteria, viruses, parasites or chemical substances [2]. *Salmonella*, as the leading risk factor for microbiological food poisoning, has been found in any link of food supply chains. However, there is still a lack of simple, rapid, sensitive and automatic methods for early screening of *Salmonella* to ensure food safety.

In the past decade, many efforts have been made to develop simple, rapid and sensitive methods for bacterial detection. Among them, the centrifugal microfluidic discs have shown great potential for separation and detection of cells, viruses and bacteria [3–8] due to low cost, less reagent, fast reaction and miniature size. In these microfluidic discs, the solutions were often transferred based on the centrifugal force owing to the rotation of the disc to perform the whole detection procedures, including transfer, mixing, capture, reaction, washing and detection, *etc.* [9–12]. An in-

* Corresponding author at: Key Laboratory of Agricultural Information Acquisition Technology, Ministry of Agriculture and Rural Affairs, China Agricultural University, Beijing 100083, China.
E-mail address: jianhan@cau.edu.cn (J. Lin).
[1] These authors contributed equally to this work.

https://doi.org/10.1016/j.cclet.2021.08.027
1001-8417/

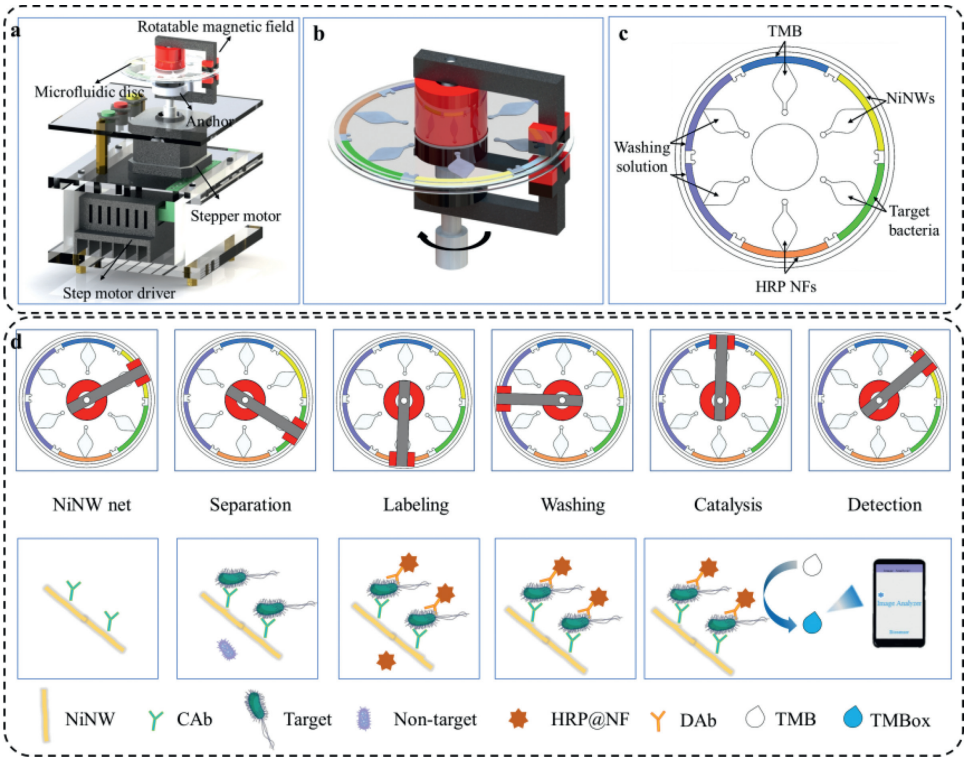

Fig. 1. (a) The lab-on-a-disc platform. (b) The rotatable magnetic field. (c) The microfluidic disc. (d) The procedure for bacterial detection.

teresting study on centrifugal microfluidic disc was reported by Nguyen *et al.* for molecular biological detection of multiple foodborne bacteria. The procedures, including sample loading, DNA extraction, LAMP reaction, and optical detection, were automatically conducted on the microfluidic disc in 1 h and it could detect *E. coli* O157: H7, *Salmonella typhimurium* and *Vibrio parahaemolyticus* with a low detection limit of 10^2 cells/mL [13]. With fast development and popularization of smartphone, it has been frequently employed to replace bulky and expensive devices for image acquisition, data analysis, result display and information transmission in the detection of foodborne pathogens [3,14–19]. Therefore, the combination of the centrifugal microfluidic disc with smartphone might be promising to provide simple, rapid and automatic methods for in-field detection of foodborne pathogens.

Signal amplification is also important for bacterial detection. Enzymes are very often used to amplify biological signals. However, their stability is limited due to their poor tolerance to harsh environment. As an alternative, some protein-inorganic hybrid nanoflowers, such as hemin-concanavalin A hybrid nanoflowers [20] and enzyme-antibody-inorganic nanoflowers [21], have been demonstrated with mimic enzyme activity and were able to greatly amplify the biological signals due to their large surface-to-volume ratio [22–26]. An interesting study was reported by Lin *et al.* using the concanavalin A-glucose oxidase-$Cu_3(PO_4)_2$ nanoflowers as HRP mimic to amplify the colorimetric signals. This method was able to detect *E. coli* O157: H7 as low as 10 CFU/mL in 3 h [27]. Therefore, the introduction of protein-inorganic hybrid nanoflowers might further improve the sensitivity of the bacterial detection methods.

In this study, a portable lab-on-a-disc platform was developed for rapid and automatic detection of *Salmonella typhimurium* using the nickel nanowire (NiNW) net to separate target bacteria from sample background, horseradish peroxidase nanoflowers (HRP NFs) to amplify biological signal, and a self-developed smartphone APP to collect and analyze colorimetric images. As shown in Fig. 1, the immune NiNWs, bacterial sample, HRP NFs, washing solution and tetramethylbenzidine (TMB) were first preloaded onto their respective chambers in the microfluidic disc and centrifuged to form multiple columns in the peripheral, which were separated by air gaps. Then, a specific magnetic field was used to assemble the NiNWs into a net, and rotated by a stepper motor to make the NiNW net successively pass through the sample column to form the NiNW-bacteria complexes (magnetic bacteria), the HRP NF column to form the NiNW-bacteria-NF complexes (nanoflower bacteria), two washing solution columns to remove the unbound HRP NFs, the TMB column to catalyze the colorless substrate (TMB) into the blue catalysate (TMBox), and the NiNW column to terminate the mimic catalysis. Finally, the image of catalysate was collected and analyzed using the self-developed smartphone APP to quantitatively determine the target bacteria.

The lab-on-a-disc platform was developed to automatically perform the whole bacterial detection procedures. As shown in Fig. 1a and Fig. S1 (Supporting information), the lab-on-a-disc platform mainly consists of a microfluidic disc, a rotatable magnetic field, a stepper motor (42BYGH34, Jiawen Electronic, Shenzhen, China), a microcontroller (STC12C5A60S2, STC, Shenzhen, China), a self-developed smartphone APP and a three-layer holder. As shown in Fig. 1b, the microfluidic disc is placed in the air gap of the magnetic field (The construction of the rotatable magnetic field can be found in Supporting information 2 and the assembly of the rotating magnetic field can be found in Video S1) at the top layer of the holder, which is automatically controlled by the stepper motor at the middle layer using the microcontroller at the bottom layer to rotate at the designated columns. The smartphone APP was developed based on Android and used to collect the image of the catalysate in the TMB column after the nanoflower bacteria were transferred to the original NiNW column and analyze the gray value of the image for quantitative determination of target bacteria.

The microfluidic disc was another key part of this lab-on-a-disc platform. As shown in Fig. 1c, the microfluidic disc consists of a top PDMS layer and a bottom glass layer. The top PDMS layer (inner diameter: 18 mm, outer diameter: 64 mm, thickness: 1.5 mm) mainly includes six inlets (diameter: 0.8 mm) for loading different solutions, six storage chambers (volume: 20 μL) for storing these solutions, six arc reaction chambers (inner diameter: 52 mm, outer diameter: 55.5 mm, height: 0.5 mm, arc angle: ∼60°) for performing separation, labeling, washing and catalysis, and twelve air holes (diameter: 0.6 mm) for positioning these columns. The design and fabrication process of the microfluidic disc can be found in Supporting information 3.

To detect unknown concentrations of target bacteria, the calibration model between the gray value of the catalysate and the concentration of the target bacteria was established. Prior to testing, the microfluidic disc was successively rinsed with 75% alcohol and deionized water, followed by blocking with 1% BSA for 30 min and washing with sterile phosphate buffered saline (PBS). First, 20 μL of the immune NiNWs (The preparation of the immune nickel nanowires can be found in Supporting information 4), 20 μL of the bacterial samples with different concentrations from 2.8×10^3 CFU/mL to 2.8×10^7 CFU/mL, 20 μL of the immune HRP NFs (The synthesis of the immune horseradish peroxidase nanoflowers can be found in Supporting information 5), 20 μL of the washing solution (PBS with 0.05% Tween 20), another 20 μL of the washing solution, and 20 μL of the TMB solution were pipetted into their respective storage chambers, respectively. Then, as shown in Video S2 (Supporting information), these solutions were centrifuged from the storage chambers to the arc reaction chambers at 700 rad/min for 3 s, resulting in the formation of one NiNW column, one sample column, one HRP NF column, two PBST columns and one TMB column, and 3 mm of air gap was formed to separate each two adjacent columns. After the microfluidic disc was placed on the platform, the magnetic field was moved by the stepper motor to the NiNW column and rotated twice from one end of the column to the other, resulting in the forming of the immune NiNW net. Then, the immune NiNW net was transferred to the sample column and rotated fifty times to separate the target bacteria, resulting in the formation of NiNW-bacteria complexes (magnetic bacteria). Successively, the magnetic bacteria were transferred to the HRP NF column and rotated fifty times, resulting in the formation of NiNW-*Salmonella*-HRP NF complexes (nanoflower bacteria). After the nanoflower bacteria were transferred to the PBST columns and rotated twenty times to remove the excessive HRP NFs, they were transferred to the TMB column and rotated thirty times, allowing efficient catalysis of colorless substrate (TMB) into blue catalysate (TMBox). Finally, the nanoflower bacteria were transferred back to the original NiNW column to terminate the catalytic reaction, and the image of catalysate was collected and analyzed by the smartphone APP to determine the target bacteria.

To verify the feasibility of this lab-on-a-disc platform for detection of target bacteria in real food samples, 25 g of the chicken meats purchased from the local supermarket were first homogenized with 225 mL of sterile PBS for 2 min using a stomacher (BagMixer CC, InterScience, Paris, France), followed by standing for 5 min to obtain the supernatant. Then, different concentrations of target bacteria were added into the supernatant to obtain the spiked chicken samples with the bacterial concentrations from 2.8×10^3 CFU/mL to 2.8×10^7 CFU/mL. Finally, the spiked chicken samples were detected using this lab-on-a-disc platform.

The formation of the NiNW net in the microfluidic channel is the key to effective separation of target bacteria from sample background, which depends on the distribution of the magnetic field since the NiNWs have the tendency to distribute along the magnetic field lines. Thus, the rotatable magnetic field was simulated using the Finite Element Method Magnetics (FEMM) software. The distribution of the rotatable magnetic field was shown in Fig. 2a, and the distribution at the air gap (from point A to point B) was shown in Fig. 2b. The magnetic field at the air gap has a mean intensity of ∼1.0 T and a mean gradient of ∼300 T/m, which was verified with the ability to form the NiNW net but without the ability to drag the NiNW net to pass through the air gaps. Thus, two repelling rectangle magnets were used to enhance the magnetic field. As shown in Figs. 2c and d, the enhanced magnetic field has a mean intensity of ∼1.4 T and a mean gradient of ∼500 T/m. When this magnetic field was applied to act on the NiNWs, the NiNWs were magnetized and observed using an electron microscope (Andonstar, Guangzhou, China) to vertically distribute in the microfluidic channel and form into the NiNW net (Fig. 2e). To better understand the forming mechanism of the NiNW net, the magnetic force on the NiNWs was investigated and shown in Fig. S2 (Supporting information). When the NiNW was in the air gap (*i.e.*, magnetic field), two magnetic forces (F_{m1} and F_{m2}) towards the direction of the higher gradient magnetic field acted on each NiNW, which had the tendency to pull the NiNW to be parallel with the magnetic field lines and thus resulted in the formation of the NiNW net across the microfluidic channel.

The nickel nanowires are the key material for the formation of the NiNW net, which is closely related with the efficiency of bacterial separation. Thus, both transmission electron microscopy (TEM) and scanning electron microscopy (SEM) were used to characterize the NiNWs. As shown in Figs. 3a and b, the NiNWs have a mean diameter of ∼180 nm and a mean length of ∼5 μm. The size of NiNWs is larger than the traditional magnetic particles, leading to easier formation of the NiNW net in the microfluidic channel.

The horseradish peroxidase nanoflowers are the key material for signal amplification, which is directly related with the sensitivity of bacterial detection. Therefore, TEM and SEM were conducted to verify successful synthesis of the HRP NFs. As shown in Figs. 3c and d, the synthesized HRP NFs have a mean diameter of ∼500 nm. The dynamic light scattering (DLS) technique was also used to further characterize the diameter of the HRP NFs, and the result in Fig. 3e verified that the diameter of the HRP NFs was ∼500 nm.

To further verify the feasibility of HRP NFs for the development of this platform, different concentrations of the HRP NFs were used to catalyze the H_2O_2-TMB substrate, followed by using the self-developed smartphone APP to collect and analyze the catalysate's image. As shown in Fig. 3f, the gray value of the catalysate decreases with the concentration of the HRP NFs, and the gray value (G) has a good linear relationship with the concentration (C_{NF}) of the HRP NFs ranging from 4 μmol/L to 500 μmol/L, which could be expressed as $G = -27.51^{*}\ln(C_{NF}) + 216.89$ ($R^2 = 0.99$), indicating that the HRP NFs could be used as detection signal.

The amount of the NiNWs, the rotating speed of the NiNW net, the times for the NiNW net to move back and forth, the amount of immune HRP NFs, and the time of enzymatic catalysis have great impact on this platform and were optimized (the optimization of the lab-on-a-disc platform can be found in Supporting information 6). As shown in Fig S3 (Supporting information), the optimal amount of 60 μg, the optimal rotating speed of 6°/s, the optimal times of 50 for the NiNW net to move in the sample, the optimal amount of 7.5 μg for the immune HRP NFs, and the optimal time of 10 min for enzymatic catalysis were obtained and used in this study.

Different concentrations of target bacteria from 2.8×10^3 CFU/mL to 2.8×10^7 CFU/mL were detected to establish the calibration model of this platform under optimal conditions. As shown in Fig. 4a, the gray value decreases from 149.1 to 97.7 when the bacterial concentration changes from 2.8×10^3 CFU/mL to 2.8×10^7 CFU/mL. A good linear relationship between gray value

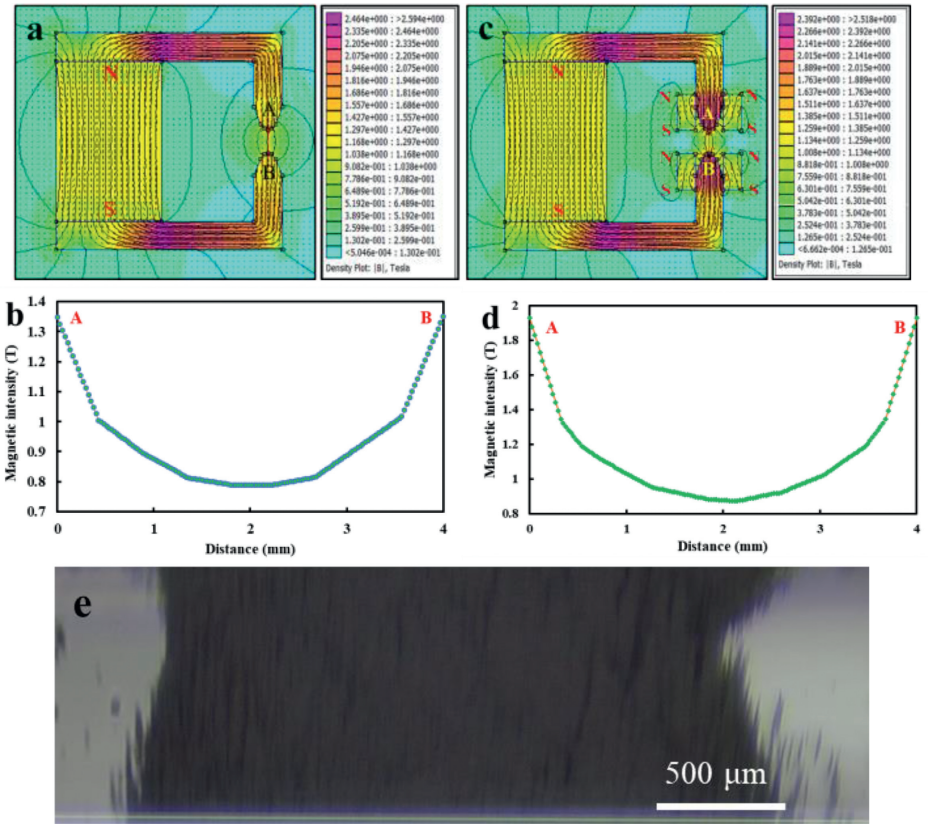

Fig. 2. (a) The simulation on the distribution of the rotatable magnetic field. (b) The vertical distribution of the magnetic field at the air gap. (c) The simulation on the distribution of the enhanced rotatable magnetic field. (d) The vertical distribution of the enhanced magnetic field at the air gap. (e) The microscopic image of the NiNW net.

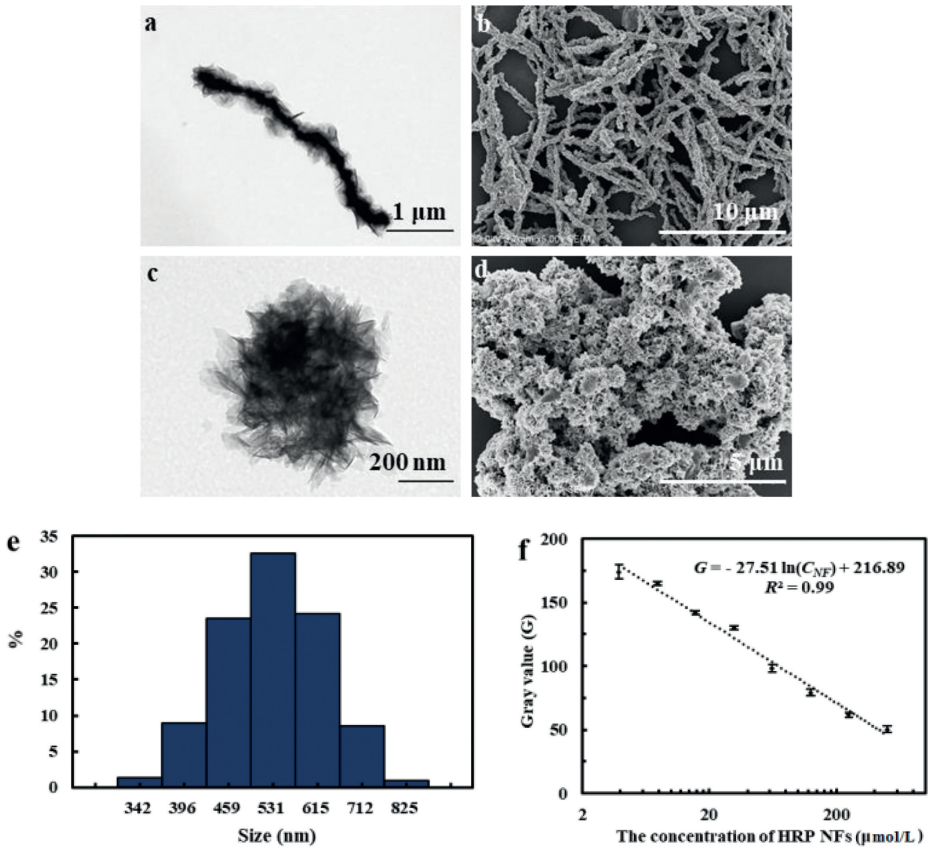

Fig. 3. (a) The TEM image of the NiNWs. (b) The SEM image of the NiNWs. (c) The TEM image of the HRP NFs. (d) The SEM image of the HRP NFs. (e) The DLS result of the HRP NFs. (f) The gray value for different concentrations of HRP NFs to catalyze the H_2O_2-TMB substrate.

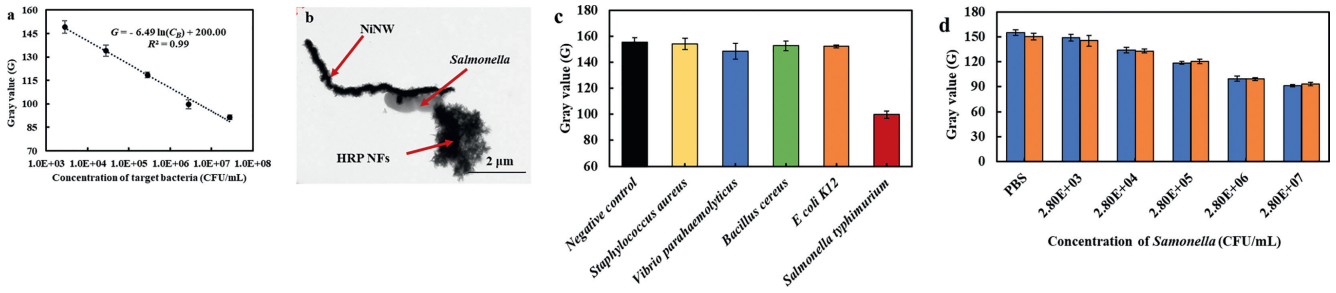

Fig. 4. (a) The calibration curve of this lab-on-a-disc platform for detection of *Salmonella* at the concentrations of 2.8×10^3–2.8×10^7 CFU/mL (N = 3). (b) The TEM image of the NiNW-*Salmonella*-NF complexes. (c) The specificity of this platform (N = 3). (d) Detection of *Salmonella* in spiked chicken meats using this platform (N = 3).

(G) and bacterial concentration (C_B) was obtained and could be described as $G = -6.49^{*}\ln(C_B) + 200.00$ ($R^2 = 0.99$). The lower detection limit for the platform was calculated to be 56 CFU/20 μL. More importantly, this platform had automatically performed the separation, labeling, washing, catalysis and detection onto the disc within 1 h. As shown in Table S1 (Supporting information), compared to some recent reported methods for bacterial detection, this platform has shown a comparable sensitivity, a simpler operation and a shorter detection time. Besides, the TEM imaging was conducted to demonstrate the formation of NiNW-*Salmonella*-NF complexes (Fig. 4b).

The specificity of this platform was evaluated by detecting three other foodborne pathogens. The experimental results on the negative control (sterile PBS buffer solution), target bacteria (*Salmonella typhimurium*) and non-target bacteria (*Staphylococcus aureus, Vibrio parahaemolyticus, Bacillus cereus* and *E. coli* K12), with the concentration of 10^6 CFU/mL were shown in Fig. 4c. The negative control and non-target bacteria show obviously higher gray values (152.7 for negative control, 154.0 for *Staphylococcus*, 148.6 for *Vibrio*, and 152.2 for *E. coli*) than the target bacteria (105.4), indicating that the platform has a good specificity.

To further evaluate the applicability of this platform for detection of *Salmonella typhimurium* in food samples, three parallel tests on different concentrations of the target *Salmonella* cells in spiked chicken meats were conducted using this platform. As shown in Fig. 4d, the recoveries for different concentrations (2.8×10^3–2.8×10^7 CFU/mL) of the target bacteria range from 97.5% to 101.8%, indicating that this platform has a good applicability for detection of *Salmonella typhimurium* in chicken meats.

In this study, a portable lab-on-a-disc platform was successfully developed for rapid and automatic detection of *Salmonella typhimurium*, and was able to quantitatively detect *Salmonella typhimurium* ranging from 5.6×10^1 CFU/20 μL to 5.6×10^5 CFU/20 μL in 1 h with the detection limit of 56 CFU/20 μL. The microfluidic disc was demonstrated to automatically and accurately distribute different reagents with air gaps through centrifugation. The NiNW net was successfully formed under the high gradient magnetic field and verified to penetrate the air gaps and pass through different columns to perform the separation, labeling, washing, catalysis and detection under the rotatable magnetic field. It is promising to be extended for on-site detection of other foodborne pathogens to ensure food safety.

Declaration of competing interest

The authors report no declarations of interest.

Acknowledgments

This research was supported by National Natural Science Foundation of China (No. 32071899) and Walmart Foundation (No. 61626817). The authors would like to thank Walmart Food Safety Collaboration Center for its great support.

Supplementary materials

Supplementary material associated with this article can be found, in the online version, at doi:10.1016/j.cclet.2021.08.027.

References

[1] The World Bank, https://www.worldbank.org/en/topic/agriculture/publication/the-safe-food-imperative-accelerating-progress-in-low-and-middle-income-countries, 2021.
[2] World Health Organization. https://www.who.int/health-topics/food-safety/, 2021.
[3] A. Sayad, F. Ibrahim, S.M. Uddin, et al., Biosens. Bioelectron. 100 (2018) 96.
[4] B.H. Park, S.J. Oh, J.H. Jung, et al., Biosens. Bioelectron. 91 (2017) 334.
[5] R. Burger, L. Amato, A. Boisen, Biosens. Bioelectron. 76 (2016) 54.
[6] M. Lim, J. Park, A.C. Lowe, et al., Theranostics 10 (2020) 5181.
[7] O. Strohmeier, S. Keil, B. Kanat, et al., RSC Adv. 5 (2015) 32144.
[8] D. Liu, Y. Zhu, N. Li, et al., Sensor Actuat. B: Chem. 310 (2020) 127834.
[9] M. Li, A. Ge, M. Liu, et al., Talanta 219 (2020) 121221.
[10] C.T. Lin, S.H. Kuo, P.H. Lin, et al., Sensor Actuat. B: Chem. 316 (2020) 128003.
[11] Y. Zhu, Y. Chen, Y. Xu, Sensor Actuat. B: Chem. 276 (2018) 313.
[12] K.D. Lenz, S. Jakhar, J.W. Chen, et al., Sci. Rep. 11 (2021) 5287.
[13] H.V. Nguyen, V.D. Nguyen, E.Y. Lee, et al., Biosens. Bioelectron. 136 (2019) 132.
[14] M.M.A. Zeinhom, Y. Wang, L. Sheng, et al., Sensor Actuat. B: Chem. 261 (2018) 75.
[15] H.V. Nguyen, V.D. Nguyen, F. Liu, et al., ACS Omega 5 (2020) 22208.
[16] Y. Man, M. Ban, A. Li, et al., Food Chem. 354 (2021) 129578.
[17] N. Cheng, Y. Song, M.M.A. Zeinhom, et al., ACS Appl. Mater. Interfaces 9 (2017) 40671.
[18] S. Shrivastava, W.I. Lee, N.E. Lee, Biosens. Bioelectron. 109 (2018) 90.
[19] J. Sun, J. Huang, Antony R. Warden, et al., Food Chem. 320 (2020) 126581.
[20] M.M.A. Zeinhom, Y. Wang, L. Sheng, et al., Sensor Actuat. B: Chem. 261 (2018) 75–82.
[21] K. Wang, S. Bu, C. Ju, et al., Bioorg. Med. Chem. Lett. 28 (2018) 3802–3807.
[22] Y. Li, H. Wu, Z. Su, Coord. Chem. Rev. 416 (2020) 213342.
[23] C. Altinkaynak, C. Gulmez, O. Atakisi, et al., Int. J. Biol. Macromol. 164 (2020) 162.
[24] N.I. Alhayali, N.K. Özpozan, S. Dayan, et al., Polyhedron 194 (2021) 114888.
[25] M. Zhang, Y. Zhang, C. Yang, et al., Talanta 224 (2021) 121840.
[26] T. Wei, D. Du, M.J. Zhu, et al., ACS Appl. Mater. Interfaces 8 (2016) 6329.
[27] R. Ye, C. Zhu, Y. Song, et al., Small 12 (2016) 3094.